ELSEVIER

Colloids and Surfaces
A: Physicochemical and Engineering Aspects 198–200 (2002) 613–623

COLLOIDS AND SURFACES A

www.elsevier.com/locate/colsurfa

Biological polyelectrolyte complexes in solution and confined on patterned surfaces

T. Pfohl [a], Y. Li [a], J.H. Kim [a,b], Z. Wen [c], G.C.L. Wong [a,1], I. Koltover [a,2], M.W. Kim [a,b], C.R. Safinya [a,*]

[a] *Materials Department, Physics Department, and Biochemistry and Molecular Biology Program, Materials Research Laboratory, University of California, Santa Barbara, CA 93106, USA*

[b] *Department of Physics, Korea Advanced Institute of Science and Technology, Taejon 305-701, South Korea*

[c] *Department of Optoelectronic Instruments, Chongqing University, Chongqing, People's Republic of China*

Received 30 August 2000; accepted 19 January 2001

Abstract

In the first part of this paper we describe recently discovered structures in self-assemblies of charged membranes complexed with the biological polyelectrolyte DNA. These complexes are currently used in medical applications of non-viral gene delivery. The second part of the paper will describe entirely new experiments where liquid crystal and biological polymers are confined on lithographically prepared patterned surfaces to produce oriented self-assemblies for structural studies and confinement induced new phases. While the focus of the paper will be on DNA, other important biological polyelectrolytes include filamentous actin (F-actin), intermediate filaments, and microtubules with varying physical and chemical molecular properties, are also discussed.

Keywords: Polyelectrolyte complexes; Patterned surfaces; Biological polymers

1. Introduction

DNA chains dissolved in solution are known to give rise to a rich variety of condensed and liquid crystalline phases at high concentrations [1,2]. Recently, there has been a flurry of experimental work on understanding the materials that are formed when DNA chains are mixed with oppositely charged cationic lipids. From a biomedical point of view, cationic liposomes (or vesicles) are empirically known to be efficient carriers of genes (i.e. sections of DNA) in synthetic gene delivery applications [3–6]. It is only recently that we are beginning to experimentally discover the new types of liquid crystalline self assembled structures in these new materials which are currently used in clinical applications [7–14].

* Corresponding author.

[1] Permanent address: Department of Materials Science and Engineering and Physics Department, University of Illinois, Urbana-Champaign, IL 61801, USA.

[2] Permanent address: Materials Science and Engineering Department, Northwestern University, Evanston, IL 60208, USA.

0927-7757/02/$ - see front matter
PII: S0927-7757(01)00978-5

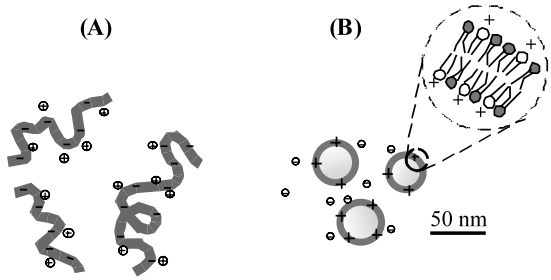

Fig. 1. (A) Linear DNA with cationic counterions condensed on the backbone due to Manning condensation. (B) Cationic liposomes (CL) (spherical membranes or vesicles) containing a bilayer of a mixture of cationic and neutral lipids (Bar for (B)).

Early on oligo-lamellar structures had been reported in cryo-TEM studies [13]. The dominant structure which forms spontaneously when DNA, a negative polyelectrolyte, is complexed with cationic liposomes (CLs) (closed bilayer shells of lipid molecules, Fig. 1) containing a specific type of lipid, is a multilayer assembly of DNA sandwiched between bilayer membranes shown schematically in Fig. 2 [7,8]. As we describe below recent quantitative synchrotron x-ray scattering [7,8] and line-shape [9,10] analysis showed that linear DNA confined between bilayers forms an

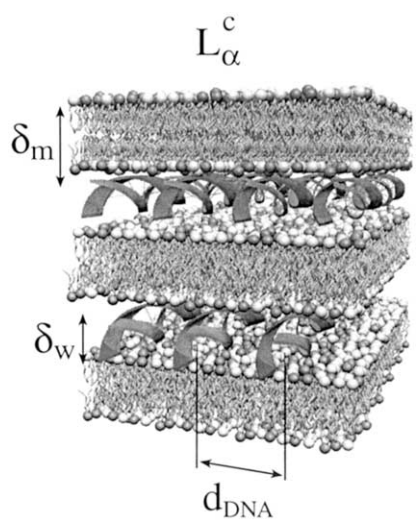

Fig. 2. Schematic of the lamellar L_α^C phase with alternating lipid bilayer–DNA monolayer of cationic lipid–DNA (CL–DNA) complexes as described in the text. The interlayer spacing is $d = \delta_w + \delta_m$ (adapted from Ref. [7]).

expanding one-dimensional (1D) lattice of chains. Thus, this phase consists of a novel 2D smectic phase resulting from long-range electrostatic repulsions. The CL–DNA complex is a new 'hybrid' phase of matter where the DNA chains form a finite size two-dimensional (2D) smectic coupled to the three-dimensional (3D) smectic lamellar phase of lipids.

The structure and thermodynamic stability of these CL–DNA complexes has also been the subject of much recent theoretical work [15–21]. Analytical and numerical studies of DNA–DNA interactions bound between membranes show the existence of a novel long-range repulsive electrostatic interaction [16–18]. Theoretical work on CL–DNA complexes has also led to the realization of a variety of novel new phases of matter in DNA–lipid complexes [20,21]. In particular, a novel new 'sliding columnar phase', which remains to be discovered experimentally, is found where the positional coherence between DNA molecules in adjacent layers is lost without destroying orientational coherence of the chains from layer to layer. This new phase would be a remarkable new phase of matter if it exists and shares many fascinating similarities with flux lattices in superconductors.

From a biophysics perspective, it is important to explore the phase behavior of DNA in two dimensions as a tractable experimental and theoretical system for understanding DNA condensation. The mechanisms of DNA condensation in vivo (i.e. packing in a small space) are poorly understood [22]. DNA condenstion and decondensation which happens, for example, during the cell-cycle in eukaryotic cells involves different types of oppositely charged polyamines, peptides and proteins (e.g. histones) where the nonspecific electrostatic interactions are clearly important. In bacteria which are the simplest cell types, it is thought that multivalent cationic polyamine molecules (spermine, spermidine) are responsible for DNA condensation in the 3D space of the cell cytoplasm. Recent experiments has led to a novel new finding where we observed attractive interactions between the DNA chains adsorbed between membranes in the presence of divalent cations leading to a DNA condensed phase in 2D [23].

The importance of the observation lies in the fact that in vitro in 3D, DNA solutions containing divalent cations exhibits the usual repulsive interactions with no hint of attractive interactions. Thus, it appears that the strength of the attractive Coulomb interactions between similarly charged polyelectrolyte rods is a strong function of either the dimension in which the rods reside or the effects of confinement.

2. Experimental details

2.1. X-ray diffraction and scattering

The quantitative in-situ measurements of the self assembled structures of membrane–biopolymer complexes were done at synchrotron sources at the Stanford Synchrotron Radiation Laboratory. The synchrotron techniques are used for the determination of both structure and interactions by measuring the material's elasticities (e.g. compression modulus and bending rigidities) derived from the inter-membrane and inter-macromolecular interactions [24–32]. We stress that, as compared to the vast experimental knowledge regarding lipid phase behavior, there is very little experimental data on membrane–bioploymer phase behavior. When needed, electron microscopic studies of freeze fractured samples were carried out.

2.2. Optical microscopy

The optical microscopy were done with video-enhanced light microscopy techniques of phase, differential interference and reflection interference contrast, together with fluorescence microscopy (Nikon inverted, Diaphot 300) [7,8,28–31].

3. Results and discussion

3.1. DNA–lipid complexes

Recent synchrotron studies [7,8] of CL–DNA complexes [where the cationic liposomes consisted of mixtures of neutral (so called 'helper-lipid') DOPC and cationic DOTAP (Fig. 3)], has revealed that the structure is different from the hypothesized 'bead-on-string' structure, originally proposed by Felgner et al. for CL–DNA complexes in their seminal paper [6], picturing the DNA strand decorated with distinctly attached cationic liposomes (refer to Fig. 1). The addition of linear λ-phage DNA (λ-DNA, 48,502 bp, contour length = 16.5 μm) to binary mixtures of cationic liposomes (mean diameter of 70 nm) induces a topological transition from liposomes into collapsed condensates in the form of optically birefringent liquid crystalline globules with size on the order of 1 μm.

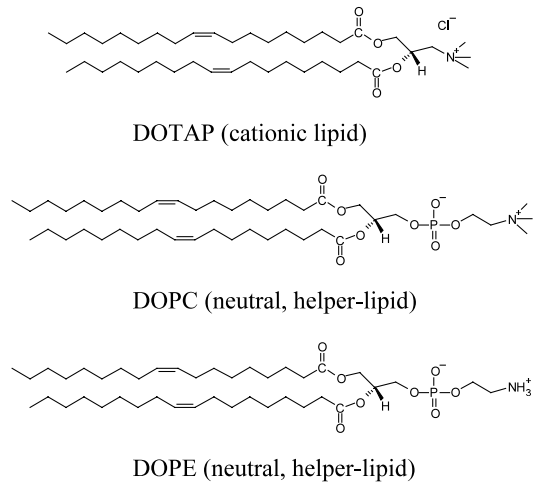

Fig. 3. Top: the cationic lipid DOTAP (dioleoyl trimethylammonium propane). Middle: the neutral helper-lipid DOPC (dioleoyl-phosphatidylcholine). Bottom: the neutral helper-lipid DOPE (dioleoyl-phosphadtidylethanolamine). The neutral lipid is referred to as the 'helper-lipid', its role will be explored in this proposal.

The small-angle-X-ray scattering (SAXS) experiments [7,8] revealed a novel self assembled structure for the condensed globules consisting of mixtures of CLs and DNA. Fig. 4 is a plot of SAXS data of λ-DNA–DOPC/DOTAP complexes as a function of increasing Φ_{DOPC} (the weight fraction of DOPC in the DOPC/DOTAP cationic liposome mixtures). The data are consistent with a complete topological rearrangement of liposomes and DNA into a multilayer structure with DNA intercalated between the bilayers (Fig.

2, denoted L_{α}^{c}). To see this we first consider complexes of DNA and DOTAP at $\Phi_{DOPC} = 0$ (Fig. 4, bottom). The two sharp peaks at $q = 0.11$ and 0.22 $Å^{-1}$ correspond to the (00L) peaks of a layered structure with an interlayer spacing d $(= \delta_m + \delta_w) = 57$ Å. The membrane thickness and water gap are denoted by δ_m and δ_w, respectively (Fig. 2).

In the absence of DNA, membranes of the cationic DOTAP exhibit strong long-range interlayer electrostatic repulsions that overwhelm the van der Waals attraction [33]. In this case, as the volume fraction Φ_w of water is increased, the L_{α} phase swells and the intermembrane distance d (which is measured by SAXS) is given by the simple geometric relation $d = \delta_m/(1 - \Phi_w)$ [33].

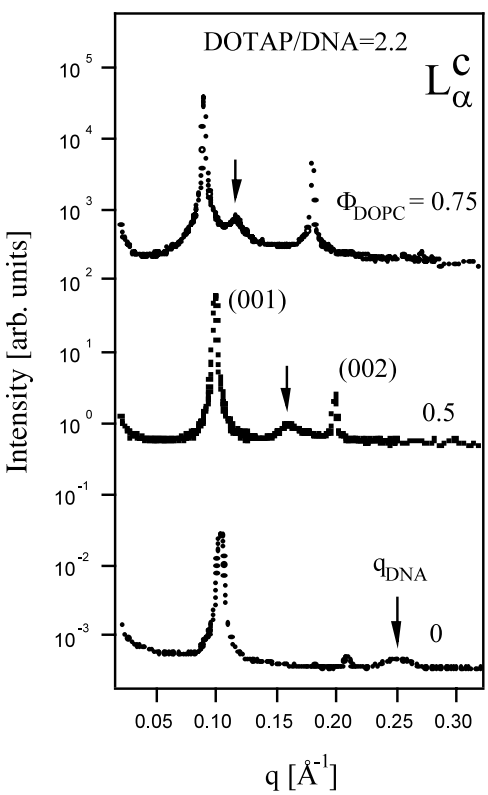

Fig. 4. SAXS scans of CL–DNA complexes at constant DOTAP/DNA = 2.2 (near the isoelectric point) with increasing DOPC/DOTAP which shows the DNA peak (arrow) moving towards smaller q, indicating that d_{DNA} increases, as L/D (and Φ_{DOPC}) increases (L = DOTAP + DOPC, D = DNA) (adapted from Ref. [7,12]).

For membranes of pure DOTAP $\delta_m = 33 \pm 1$ Å [7,8]. Highly dilute liposomes of DOTAP (with $\Phi_w \approx 98.5\%$ used in the SAXS experiments) do not exhibit Bragg diffraction in the small wavevector range covered in Fig. 4. Thus, the DNA that condenses on the cationic membranes strongly screens the electrostatic interaction between lipid bilayers and leads to condensed multilayers. The average thickness of the water gap $\delta_w = d - \delta_m = 57–33$ Å $= 24 \pm 1$ Å is just sufficient to accommodate one monolayer of B-DNA (diameter20 Å) including a hydration shell [34]. As we now discuss the broad peak denoted $q_{DNA} = 0.256$ $Å^{-1}$ arises from DNA–DNA correlations and gives $d_{DNA} = 2\pi/q_{DNA} = 24.55$ Å (Fig. 2).

The precise nature of the packing structure of λ-DNA within the lipid layers can be elucidated by conducting a lipid dilution experiment in the isoelectric point regime of the complex. In these experiments the total lipid (L = DOTAP + DOPC) is increased while the charge of the overall complex, given by the ratio of cationic DOTAP to DNA, is kept constant at the isoelectric point DOTAP/DNA = 2.20. The SAXS scans in Fig. 4, (arrows point to the DNA peak) show that $d_{DNA} = 2\pi/q_{DNA}$ increases with lipid dilution from 24.54 to 57.1 Å as Φ_{DOPC} increases from 0 to 0.75 (or equivalently increasing L/D between 2.2 and 8.8). The most compressed interaxial spacing of ≈ 24.55 Å at $\Phi_{DOPC} = 0$ approaches the short-range repulsive hard-core interaction of the B-DNA rods containing a hydration layer [34]. Fig. 5(A) plots d and d_{DNA} as a function L/D.

The observed behavior is depicted schematically in Fig. 5(B) showing that as we add neutral lipid (at the isoelectric point) and therefore expand the total cationic surface we expect the DNA chains to also expand and increase their interaxial spacing. The solid line in Fig. 5(A) is derived from the simple geometric packing relationship $d_{DNA} = (A_D/\delta_m)(\rho_D/\rho_L)$ (L/D) which equates the cationic charge density (due to the mixture $DOTAP^{+}$ and DOPC) with the anionic charge density (due to DNA^{-}) and is only valid at the isoelectric point where there is no excess lipid or DNA coexisting with the complex [7,8]. Here, $\rho_D = 1.7$ (g/cc) and $\rho_L = 1.07$ (g/cc) denote the densities of DNA and

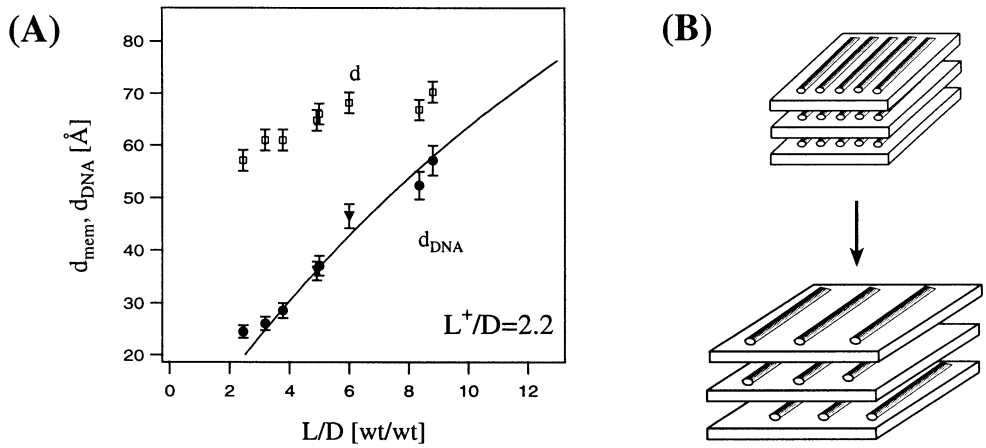

Fig. 5. (A) The DNA interaxial distance d_{DNA} and the interlayer distance d in the L_α^c phase (Fig. 2) plotted as a function of lipid/DNA (L/D) (wt./wt.) ratio at the isoelectric point of the complex DOTAP/DNA = 2.2. d_{DNA} is seen to expand from 24.5 to 57.1 Å. The solid line through the data is the prediction of a packing calculation where the DNA chains form a space filling one-dimensional lattice. (B) Schematic of DNA-membrane multilayers showing the increase in distance between DNA chains as the membrane charge density is decreased (as Φ_{DOPC} increases) at the isoelectric point (adapted from Refs. [7,12]).

lipid respectively, δ_m the membrane thickness, and A_D the DNA area. $A_D = Wt(\lambda)/(\rho_D L(\lambda)) = 186$ Å^2, $Wt(\lambda)$ = weight of λ-DNA = $31.5 \times 10^6/(6.022 \times 10^{23})$ g and $L(\lambda)$ = contour length of λ-DNA = 48502×3.4 Å. The agreement between the packing relationship (solid line) with the data over the measured interaxial distance from 24.55 to 57.1 Å (Fig. 5(A)) is quite remarkable given the fact that there are no adjustable parameters. The variation in the interlayer spacing d ($= \delta_w + \delta_m$) (Fig. 5(A), open squares) arises from the increase in the membrane bilayer thickness δ_m as L/D increases (each DOPC molecule is about 4–6 Å longer than a DOTAP molecule). The observation, of a variation in the DNA interaxial distance as a function of the lipid to DNA (L/D) ratio in multilayers (Fig. 5(A)), unambiguously demonstrates that X-ray diffraction directly probes the DNA behavior in multilayer assemblies [7,8]. From the linewidths of the DNA peaks the 1D lattice of DNA chains is found to consist of domains extending to near ten neighboring chains [9,10]. Thus, the DNA chains form a finite-sized 1D ordered array adsorbed between 2D membranes; that is, a finite sized 2D smectic phase of matter. On larger length scales the lattice would melt into a 2D nematic phase of chains due to dislocations.

The DNA–lipid condensation can be understood to occur as a result of release of 'bound' counterions in solution. DNA in solution (Fig. 1) has a bare length between negative charges (phosphate groups) equal to $b_o = 1.7$ Å. This is substantially less than the Bjerrum length in water $bj = 7.1$ Å which corresponds to the distance where the Coulomb energy between two unit charges is equal to the thermal energy k_BT. A non-linear Poisson–Boltzmann analysis shows that counterions will condense on the DNA backbone until the Manning parameter $\xi = bj/b'$ approaches 1 [35]. (b' is the renormalized distance between negative charges after counterion condensation.) A similar analysis shows that counterions also condense near the surface of 2D membranes (i.e. within the Gouy–Chapman layer) [36]. Through DNA–lipid condensation the cationic lipid tends to fully neutralize the phosphate groups on the DNA in effect replacing and releasing the originally condensed counterions in solution. Thus, the driving force for higher-order-self-assembly is the release of counterions, which were one-dimensionally bound to DNA and two-dimensionally bound to cationic membranes, into solution.

3.1.1. The role of the 'helper-lipid' and cationic lipid in controlling the interaction free energy in cationic lipid–polyelectrolyte biopolymer complexes

We have recently observed a transition from the L_α^C to the inverted hexagonal H_{II}^C (Fig. 6) structure in CL–DNA complexes containing DOTAP and DOPE as a function of increasing Φ_{DOPE} [11]. The transition can be understood by noting that in contrast to the helper-lipid DOPC and the cationic lipid DOTAP (Fig. 3) which have a zero natural curvature ($C_o^{DOTAP,DOPC} = 1/R_o^{DOTAP,DOPC} = 0$), DOPE is cone-shaped with $C_o^{DOPE} = 1/R_o^{DOPE} < 0$. Thus, the natural curvature of the monolayer mixture of DOTAP and DOPE is driven negative with $C_o = 1/R_o = \Phi_{DOPE} C_o^{DOPE}$. Hence, as a function of increasing Φ_{DOPE} we expect a transition to the H_{II}^C phase favored by the elastic free energy as the data indicate (Fig. 6). The helper-lipid DOPE appears to induce the L_α^C to H_{II}^C transition by controlling the spontaneous radius of curvature R_o of the lipid layers [11].

The L_α^C to H_{II}^C transition can also occur along a different path by reducing the bending rigidity κ of the lipid layer and thus the membrane elastic energy which prevents the formation of the H_{II}^C phase theoretically assumed to be favored by electrostatics [11].

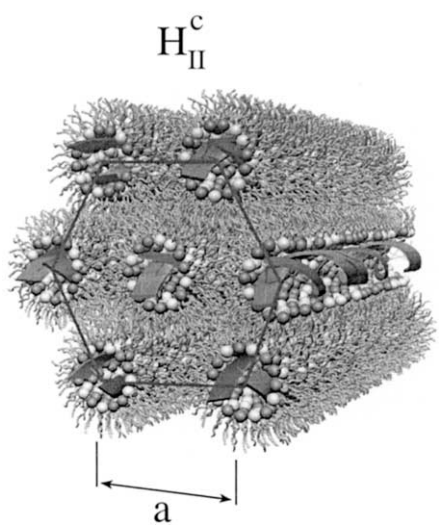

Fig. 6. Schematic of the inverted hexagonal H_{II}^C phase (cylinders consisting of DNA coated with a lipid monolayer arranged on a hexagonal lattice) of cationic lipid–DNA (CL–DNA) complexes (adapted from Ref. [11]).

3.2. Biomolecular materials self-assembled on micro- and nano-scale patterned surfaces: orientation, and technological applications

To obtain oriented phases and confinement-induced new phases consisting of the membranes complexed with polyelectrolyte biopolymers we have recently developed methods for producing and characterizing the structures in such biomolecular materials self-assembled on patterned (linear channels, both varying and constant channel width) surfaces. These patterned surfaces are produced by using optical and electron-beam lithography and wet (HF) or dry (reactive ion) etching methods for fabrication of 10s of microns to about 100 nanometer features. The electron-beam based microchannels are produced at the UCSB branch of the National Nanofabrication Users Network. Scanning electron microscopy is used to characterize and monitor for imperfections. We have fabricated linear width microchannels with widths ranging between 20 μm down to 100 nm on a variety of substrates (Si, GaAs, (100 μm thick wafers) and glass plates (170 μm thick)). Channel depths may be as small as 2 nm (i.e. the etch resolution) and as large as five to ten times deeper than the width but in typical cases is about 1.5 μm. These will be used for structural studies of biomolecules mixed in micron and sub-micron scale microchannel structures as substrate matrices for confining, orienting, and guiding the growth direction of the self assemblies.

A scanning electron microscope (SEM) image of a 5 μm wide and 1 μm deep channel is shown in Fig. 7 (TOP). The patterned surface consisting of channel arrays were chemically (HF) etched onto the smooth (100) Si substrates after patterning by photolithography using a custom-designed mask. Each channel array has an area of 1 mm × 1 mm and consists of periodic 1 mm long linear channels with uniform channel width ranging from 1.5 to 20 μm. The depth of the channels was measured to be between 1 and 7 μm. Using recently developed methods the patterned surfaces

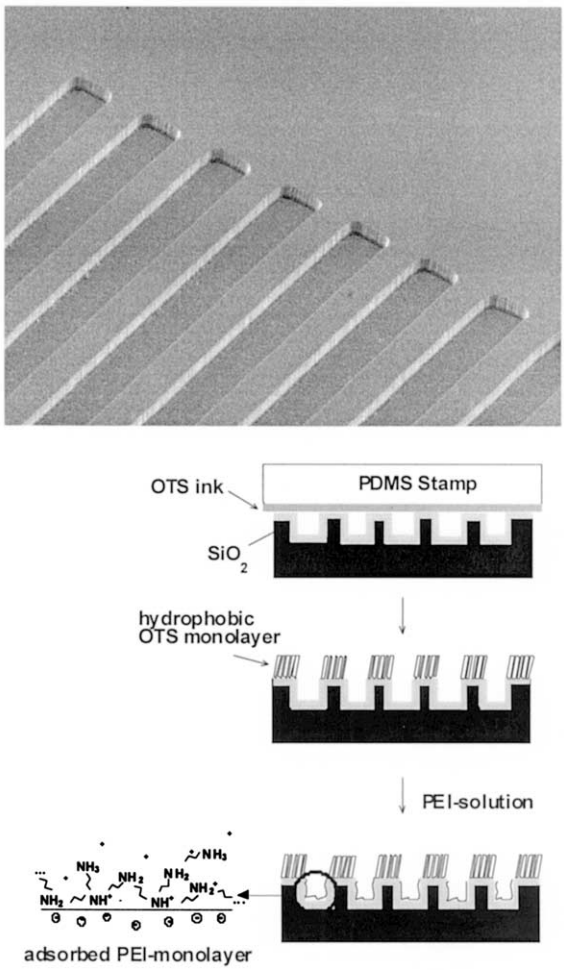

Fig. 7. Top: scanning electron microscope (SEM) image of a patterned surface consisting of 5 μm wide channel arrays. The depth of the channels is ~1 μm. Bottom: one of the two surface modification procedures used to create wetting contrast in the channels. The treated channels are hydrophobic on the top and hydrophilic inside, which facilitates loading and processing of biomaterials in the channels.

are typically modified so that the valleys (grooves) are hydrophilic while the top surfaces are hydrophobic. In this manner the charged membrane–polyelectrolyte biopolymer complex remains inside the grooves. Typically the entire pattern is initially rendered hydrophilic by a standard RCA method using a mixture of 30% H_2O_2, 30% NH^{3+}, H_2O (1:1: 5) which leaves both hydroxyl and O^- groups on the surface. Next a 37% HCl and water mixture (1:1) converts most of the O^- groups into hydroxyl groups. One method that we have developed to achieve this is based on the use of microcontact printing and polyelectrolyte absorption, which is schematically depicted in Fig. 7 (bottom). In this process, a flat microcontact stamp made from poly(dimethylsiloxane) (PDMS) was first used to ink the top surfaces of the channels with a dry hexane solution of octadecyltrichlorosilane (OTS), which is covalently bound to the natural SiO_2 layer and thus making the surface hydrophobic. After proper washing in ethanol and water to remove extra ink, the channels were immersed in an aqueous solution of positively charged 750,000 molecular weight poly(ethylene imine) (PEI). After proper washing, the channel walls are left with only a hydrophilic PEI monolayer, which is bound to the channel walls by electrostatic interactions (the channel walls and bottom are negatively charged due to dangling bonds at the surface of the SiO_2 layer). Alternatively, the substrates can be coated with PEI first (this include the top surfaces of the channels) and then a hydrophobic OTS layer is then stamped on the top surfaces, with OTS bonding to alkylsilanes chemisorbed on the PEI monolayer.

For our initial studies we chose to use a liquid crystal system as a model system. The influence of the confinement of the micro-scale fluids on material properties has been shown for the thermotropic liquid crystal 8CB (4′-*n*-octyl-4-cyanobiphenyl). The liquid crystal 8CB consists of rod-shaped molecules which have a permanent dipole moment at one end due to their cyano-group. The individual molecules have a length of around 2.3 nm. In the varoius liquid crystal phases the molecules form anti-parallel dimers of length 3.2 nm. At temperatures above 40.5 °C 8CB is in the isotropic phase. Between 40 and 33.5 °C the material is in the nematic phase which has long range orientational order with the rod-shaped molecules all pointed on average in the same direction. The molecules, however, exhibit liquid-like positional order. Below 33.5 °C, the material undergoes a phase transition to the smectic A phase where the rod-shaped molecules segregate into stacks of liquid-like layers forming a one-dimensional density wave.

We show that we can control the rheological properties (i.e. the elastic and viscous parameters) of the thin liquid crystal fluid by controlling the mesoscale defect structure through the variation of the width of the microchannels (Fig. 8). The manipulation of a single microchannel provides a promising technique for producing nano- to microscale fluid films under well controlled geometries and will also allow us to study and clarify, their wetting and rheological properties at the nanometer to 100 s of nanometer length scales.

The polarized microscopy images in Fig. 8(A) show the liquid crystal in the nematic phase. The thread-like texture of the nematic phase can be clearly seen. The confining 20 μm width of the microchannels leads to a defect structure on a much smaller length scale than in bulk liquid crystal films. Upon cooling the samples in microchannels from the nematic phase (Fig. 8(A)) to the smectic-A phase a novel defect structure of the confined smectic A phase was observed (Fig. 8(B)). This structure consisted of a collection of distorted spherulite-like domains in which the layers of the liquid crystal molecules are aligned in onion-like distorted concentric spheres. Spherulites are a particular type of defect structures with positive Gaussian curvature. Some classical focal conic defects (where the layers form a torus-like structure) with negative Gaussian curvature are also evident. The size distributions of the spherulite domains in these 20 μm microchannels, while not perfectly monodisperse, already show the effects of confinement and are surprisingly not too polydisperse. When the channel width is reduced down to 3 μm (data to be published), we have found a surprisingly different texture in the smectic A phase in which the defects adapt a perfectly monodisperse uniform size which is controlled by the channel width.

Thus, through confinement on a mesoscale, the defect structure and the size of this structure of the liquid crystal with much smaller molecule dimensions can be manipulated and controlled. These different defect structures are known to result in a large change in material properties; for example, the rheological (elastic and viscous) properties. The use of geometric constraints for the control of the mesoscopic structure and material properties may be transferred to other materials such as block copolymers.

Highly oriented biomolecules can be prepared by using the microchannels as substrates. In Fig. 9, two polarized optical microscopy images are shown for a microchannel filled with calf thymus DNA solutions. The sample was prepared by

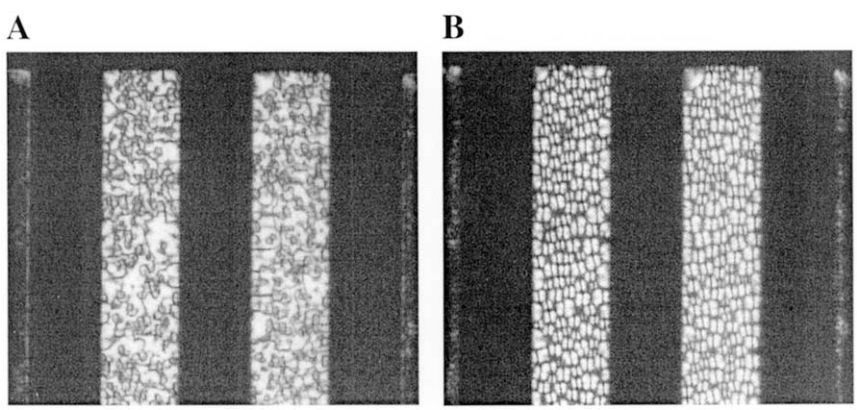

Fig. 8. The liquid crystal 8CB confined on microstructured surfaces. The figure shows confinement of the fluid in microchannels with width 20 μm viewed between crossed polarizers. (A) The micrograph shows the defect structure of 8CB in the nematic phase. (B) The micrograph shows the defect structure of the confined 8CB in the smectic A phase. Note the novel spherulite-like defect structure with a relatively small polydispersity of size.

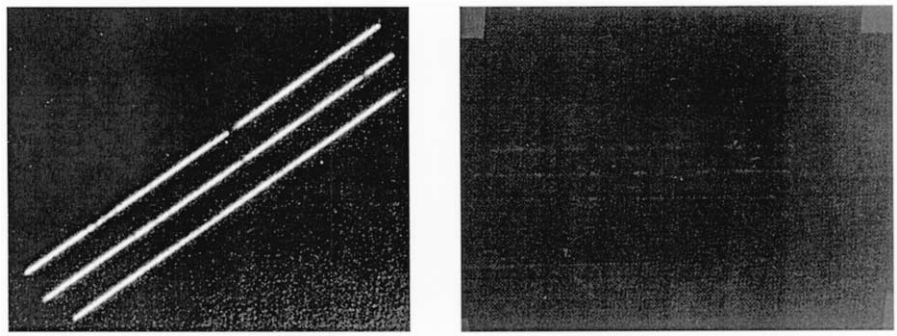

Fig. 9. Polarized microscopy images of microchannels filled with calf thymus DNA directly deposited using a microinjection system. The extinction of light under crossed polarizers (B) indicates that the DNA molecules are aligned along the channels.

repeated filling of channels of the dilute DNA solution and let the water evaporate, thus forming a highly concentrated DNA sample. The near complete extinction of the light on the image (B) which was taken with the sample rotated by 45° with respect to the image on the left (A) suggests linear alignment of the DNA molecules along the channel direction. The alignment was induced both by geometric confinement, as the channel width (in this case 1.5 μm) approaches the characteristic size of the biomolecule (e.g. radius of gyration, persistent length), and by capillary flow inside the channel when it was filled with the microinjector. Preparing highly oriented samples is crucial to many studies investigating the structures of biological macromolecules using optical microscopy and X-ray diffraction. The most common methods used presently include orienting these samples in magnetic field, capillary flow and shear apparatus. The results we obtained with DNA, microtubules and F-Actin, demonstrated that the microfluidic channel arrays are very effective substrates for aligning these molecules. However, due to the finite thickness and width of the samples which was set by the channel depth and width, it would be difficult to extract sufficient signal using convention X-ray diffraction methods. We are currently developing X-ray micro-diffraction methods utilizing a linearly focused X-ray beam with a focus size smaller than the channel width, which would be ideally suited for structural investigations using the microchannel arrays.

4. Future directions

The biopolymers which we are currently exploring include DNA, F-actin, and microtubules. We expect the persistence length to be a critical parameter in achieving oriented biopolymers adsorbed onto membranes. The surfactant bilayers are expected to be oriented by the influence of the bottom surface and temperature annealing independent of the width of the channels. As we show schematically in Fig. 10(b), we expect the biopolymer should exhibit orientational order when the persistence length exceeds the width of the confining channels. Thus, our choice of biopolymers with different persistence lengths (1000 Å for DNA, 2–5 microns for F-action, and much larger for microtubules) will allow us to test this idea. These experiments should lead to the possiblity of observing new phases [37] and, in particular, a novel 'confinement induced' sliding columnar phase predicted by recent theory where the biopolymers are orientationally locked (but positionally disordered) from layer to layer [20,21]. Future microdiffraction X-ray studies [38,39] (using either Bragg–Fresnel lenses or transmission zone-plate focusing optics) of samples oriented due to confinement in microchannels will allow an independent measurement of κ_c and will open up a novel new way to determine the persistence length of surface adsorbed polyelectrolytes.

Aside from the structural studies, the oriented multilamellar structure would have many important technological applications. These oriented

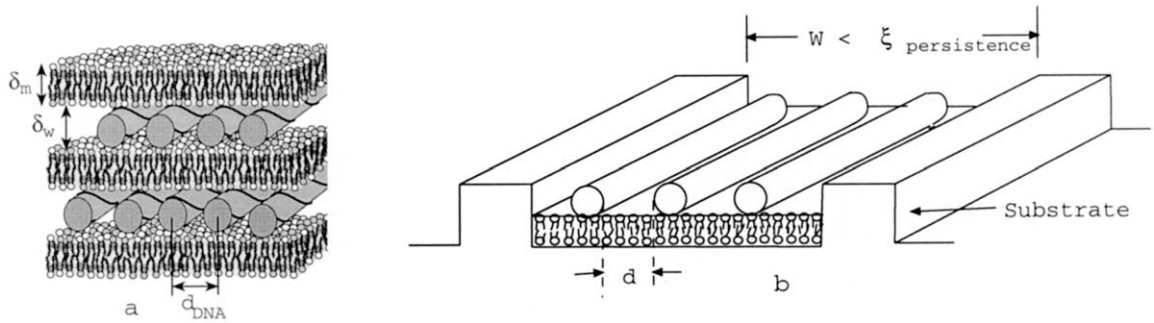

Fig. 10. (a) Schematic of the multilamellar structure of CL–polyelectrolyte bioploymer (DNA, F-actin, or microtubule) complexes with alternating lipid bilayer and polyelectrolyte multilayer. (b) Proposed experiment with polyelectrolyte bioploymer-membrane oriented in microchannels for structural studies and with applications in nanolithography and separations. Both thick multilayer and ultrathin layers can be studied.

bioploymer/multilamellar structures confined in microchannels will be used to produce nanoscale materials. In one set of experiments we will use the anionic biopolymer (DNA, microtubule, F-actin) as a template for adsorbing divalent cations on the route to producing nano-wires. In recent experiments on unoriented bulk samples we have found that in the presence of divalent cations (e.g. Mg^{2+}, Co^{2+}) the DNA lattice adsorbed on membranes undergoes a condensation transition with the DNA interchain spacing abruptly collapsing to 28 Å and the divalent cations electrostatically bound to and trapped between neighboring DNA chains (Fig. 10) [23]. Once the divalent cations are bound to the DNA template, two different reaction routes can be followed to form the desired chemical reactions leading to nanoscale wires with conducting or semiconducting properties. The first involves saturation in a chalcongenide gas (e.g. H_2S), and the second involves a reduction reaction (basic hydroquinone/OH^- solution) followed by an acidic reaction of hydroquinone/H^+ and cations [40].

5. Uncited reference

[32]

Acknowledgements

We gratefully acknowledge useful discussions with Karlheinz Graf, Thilo Pompe, Ralf Seemann, Markus Seitz and Nelle Slack. We especially acknowledge many discussions on confined fluid films with Jacob Israelachvili. We thank Gernot Wirnsberger for the help with the preparation of structured PDMS stamps. This research was supported by National Science Foundation Grants DMR-9972246 and DMR-0076357, National Institutes of Health Grant GM59288, ONR-N00014-00-1-0214, and the University of California Biotech Research, and Education Program Training Grant 99-14. The Materials Research Laboratory at UC-Santa Barbara is supported by NSF-DMR-0080034. TP acknowledges the support by a DFG (Pf 375/1-1) scholarship. MWK acknowledges the partial support by KISTEP (99-I-01-03-A-064).

References

[1] See e.g. V.A. Bloomfield, Biopolymers 31 (1991) 1471.
[2] See e.g. F. Livolant, A. Leforestier, Prog. Poly. Sci. 21 (1996) 1115.
[3] For a recent review see e.g. S. Chesnoy, L. Huang, Annu. Rev. Biophys. Biomol. Struct. 29 (2000) 27.
[4] A.D. Miller, Angew. Chem. Int. Ed. Engl. 37 (1998) 1768.
[5] T. Friedmann, Sci. Am. 276 (1997) 96.
[6] P.L. Felgner, T.R. Gadek, M. Holm, R. Roman, H.W. Chan, M. Wenz, J.P. Northrop, G.M. Ringold, M. Danielsen, Proc. Natl. Acad. Sci. USA 84 (1987) 7413.
[7] J.O. Raedler, I. Koltover, T. Salditt, C.R. Safinya, Science 275 (1997) 810.
[8] J.O. Raedler, I. Koltover, T. Salditt, A. Jamieson, C.R. Safinya, Langmuir 14 (1998) 4272.
[9] T. Salditt, I. Koltover, J.O. Raedler, C.R. Safinya, Phys. Rev. Lett. 79 (1997) 2582.

[10] T. Salditt, I. Koltover, J.O. Raedler, C.R. Safinya, Phys. Rev. E 58 (1998) 889.
[11] I. Koltover, T. Salditt, J.O. Raedler, C.R. Safinya, Science 281 (1998) 78.
[12] I. Koltover, T. Salditt, C.R. Safinya, Biophys. J. 77 (2) (1999) 915.
[13] J. Gustafsson, G. Arvidson, G. Karlsson, M. Almgren, Biochim. Biophys. Acta Biochem. 1235 (1995) 305.
[14] D.D. Lasic, H.H. Strey, M.C.A. Stuart, R. Podgornik, P.M. Frederik, J. Am. Chem. Soc. 119 (1997) 832.
[15] S. May, A. Ben-Shaul, Biophys. J. 73 (1997) 2427.
[16] N. Dan, Biochim. Biophys. Acta 1369 (1998) 34.
[17] R. Bruinsma, Eur. Phys. J. B 4 (1998) 75.
[18] R. Bruinsma, J. Mashl, Europhys. Lett. 41 (2) (1998) 165.
[19] D. Harries, S. May, W.M. Gelbart, A. Ben-Shaul, Biophys. J. 75 (1998) 159.
[20] C.S. O'Hern, T.C. Lubensky, Phys. Rev. Lett. 80 (1998) 4345.
[21] L. Golubovic, M. Golubovic, Phys. Rev. Lett. 80 (1998) 4341.
[22] B. Lewin, Genes VI, Oxford University Press, Oxford, 1997.
[23] I. Koltover, K. Wagner, C.R. Safinya, Proc. Natl. Acad. Sci. USA 97 (2000) 14046.
[24] C.R. Safinya, Colloids Surf. A Physiochem. Eng. Aspects 128 (1-3) (1997) 183.
[25] C.R. Safinya, E.B. Sirota, D. Roux, G.S. Smith, Phys. Rev. Lett. 62 (1989) 1134.
[26] G.S. Smith, E.B. Sirota, C.R. Safinya, N.A. Clark, J. Chem. Phys. 92 (1990) 4519.
[27] D. Roux, C.R. Safinya, F. Nallet, in: A. Ben-Shaul, W.M. Gelbart, D. Roux (Eds.), Micelles, Membranes, Microemulsions and Monolayers, Ch. 6, Springer-Verlag, New York, 1994, pp. 303–338.
[28] H.E. Warriner, S.H.J. Idziak, N.L. Slack, P. Davidson, C.R. Safinya, Science 271 (1996) 969.
[29] S. Chiruvolu, H.E. Warriner, E. Naranjo, K. Kraiser, S.H.J. Idziak, J. Radler, R.J. Plano, J.A. Zasadzinski, C.R. Safinya, Science 266 (1994) 1222.
[30] B.N. Thomas, C.R. Safinya, R.J. Plano, N.A. Clark, Science 267 (1995) 1635.
[31] C.F. Schmidt, K. Svoboda, N. Lei, I. Petsche, L. Berman, C.R. Safinya, G.S. Grest, Science 259 (1993) 952.
[32] Yi. Shen, C.R. Safinya, K.S. Liang, A.F. Ruppert, K.J. Rothschild, Nature 366 (1993) 48.
[33] D. Roux, C.R. Safinya, J. Phys. (France) 49 (1988) 307.
[34] R. Podgornik, D.C. Rau, V.A. Parsegian, Biophys. J. 66 (1994) 962.
[35] G.S. Manning, J. Chem. Phys. 51 (1969) 924.
[36] M. LeBret, B.H. Zimm, Bioploymers 23 (1984) 287.
[37] G.C.L. Wong, J.X. Tang, A. Lin, Y. Li, P.A. Janmey, C.R. Safinya, Science 288 (2000) 2035.
[38] Y. Li, G.C.L. Wong, C.R. Safinya, E.J. Caine, E.L. Hu, D. Haeffner, P. Fernandez, W. Yun, Rev. Sci. Instrum. 69 (8) (1998) 2844.
[39] Y. Li, G.C.L. Wong, R. Case, C.R. Safinya, E.J. Caine, E.L. Hu, D. Haeffner, P. Fernandez, Appl. Phys. Lett. 77 (3) (2000) 313.
[40] See e.g. P.V. Braun, P. Osenar, S.I. Stupp, Nature 380 (1996) 325.